

Topological Fermi-surface Reconstruction in the Repulsive Fermi-Hubbard Model

Ian Osborne¹, Thereza Paiva², and Nandini Trivedi¹

(1) *Department of Physics, The Ohio State University, Columbus, OH 43210, USA and*

(2) *Instituto de Física, Universidade Federal do Rio de Janeiro, Caixa Postal 68.528, 21941- we 972, Rio de Janeiro, RJ, Brazil*

(Dated: July 28, 2022)

One of the fundamental questions about the high temperature cuprate superconductors is the size of the Fermi surface (FS) underlying the superconducting state. By analyzing the single particle spectral function for the Fermi Hubbard model as a function of repulsion U and chemical potential μ , we find that the Fermi surface reconstructs from a large Fermi surface enclosing $(1+p)$ holes, matching the Luttinger volume as expected in a Fermi liquid, to a small Fermi surface enclosing closer to p holes. This transition into a non-Fermi liquid phase, dubbed the FL* phase with topological order, occurs as the Mott insulator at half filling is approached, in the absence of any other broken symmetry. We obtain the Fermi surface contour from the spectral weight $A_{\vec{k}}(\omega=0)$ and the retarded Green's function, $G_{\vec{k}}^{ret}(E=0)=0$, calculated using determinantal quantum Monte Carlo and analytic continuation methods. We discuss our numerical results in connection with experiments on Hall measurements, scanning tunneling spectroscopy and angle resolved photoemission spectroscopy.

Introduction: A question of fundamental importance for strongly correlated metals near a Mott transition is: What is the size of the Fermi surface? Does it count all the electrons or only the carriers relative to the Mott filling? In other words, is the Fermi surface large or small? And furthermore, if the Fermi surface deviates from the Luttinger volume and there is Fermi surface reconstruction, is it due to competing order or due to topological order?

We are motivated by three sets of experiments on the cuprates: The Hall coefficient which gives information on the density and type of carriers, scanning tunneling spectroscopy that gives information about broken charge density and pair density order, and angle resolved photoemission spectroscopy that gives information about the momentum resolved density of states. The Hall number n_H in $\text{YBa}_2\text{Cu}_3\text{O}_y$ (YBCO) shows a distinct change from $n_H \approx 1+p$ at high doping p of holes to $n_H \approx p$ for low doping at a critical p_c^H .¹ The next question is whether the change in behavior of the Hall coefficient occurs due to broken symmetry in the charge, spin or pairing channel. Scanning tunneling spectroscopy experiments indicate that charge order is observed in YBCO below a critical doping $p_c^{CDW} < p_c^H$, which suggests that the mechanism causing the change of the Hall coefficient and the mechanism driving charge order are distinct phenomena.

Here we sharpen the question for the celebrated Hubbard model rather than focusing on analysis of experiments; the latter being undoubtedly more complicated. Early QMC calculations of the spectral function related antiferromagnetic fluctuations to pseudogap formation and quasiparticle weight transfer²⁻⁵. More recent work focused on systems with particle-hole asymmetry, introduced by next-near neighbour hopping. Cluster Dynamical Mean-Field (CDMFT) studies have shown that the quasi-particles show momentum-dependent renormalizations due to proximity to the Mott transition, even in the absence of long-ranged antiferromagnetic correla-

tions.⁶⁻¹⁰

In this paper, our aim is to extract the underlying Fermi surface as a function of doping, with particular emphasis on the region close to the Mott transition⁷. Using determinantal quantum Monte Carlo methods we obtain the imaginary time Green function, $G_{\vec{k}}(\tau)$ as a function of the interaction strength, carrier concentration and temperature. Analytic continuation of G yields the spectral function $A_{\vec{k}}(\omega)$ ¹¹⁻¹⁴ whose contour at $\omega=0$ yields the Fermi surface. Remarkably, we find evidence for Fermi surface reconstruction in the absence of any competing order, indicating the emergence of topological order close to the Mott transition.¹⁵

Models and Methods: The Fermi Hubbard model is the paradigmatic model for Mott insulators, strongly correlated metals, and high temperature superconductors. In its particle-hole symmetric form, the Hamiltonian is given by

$$\mathcal{H} = -t \sum_{\langle i,j \rangle, \sigma} \left(\hat{c}_{i,\sigma}^\dagger \hat{c}_{j,\sigma} + h.c. \right) + U \sum_i \left(\hat{n}_{i\uparrow} - \frac{1}{2} \right) \left(\hat{n}_{i\downarrow} - \frac{1}{2} \right) - \mu \hat{N} \quad (1)$$

defined so that when the chemical potential $\mu=0$, the average density is unity ensuring that the system is half-filled. Here t is the tunneling amplitude for a fermion to hop from one site to a neighbor without changing the spin $\sigma = \uparrow, \downarrow$, and U is the on-site Coulomb repulsion. The spatial index i labels a site on a 2D square lattice, and $\hat{c}_{i,\sigma}$ and $\hat{c}_{i,\sigma}^\dagger$ are fermionic annihilation and creation operators respectively. The number operator is defined as $\hat{n}_{i,\sigma} \equiv \hat{c}_{i,\sigma}^\dagger \hat{c}_{i,\sigma}$, $\hat{n}_i = \hat{n}_{i,\uparrow} + \hat{n}_{i,\downarrow}$, and the particle density per site $n = \sum_i \langle \hat{n}_i \rangle / N_s$, where N_s is the total number of sites. Relative to the filled band with two electrons per site, the hole density is $1+p$. Particle-hole symmetry is exhibited by the transformation of particle creation and

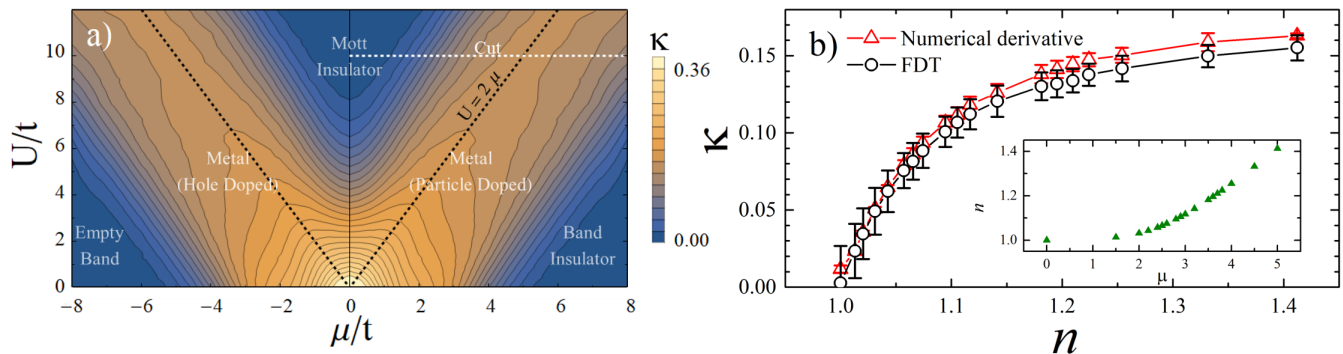


FIG. 1. a) Compressibility κ is calculated on a 6×6 lattice as a function of interaction potential (U) and chemical potential (μ) at $\beta t = 2$ in units of $(tN_s)^{-1}$, where N_s is the number of sites. Small (close to zero) compressibility (blue) indicates Mott and band insulating phases; positive compressibility corresponds to a metallic phase. b) Compressibility κ is calculated for a 16×16 system with a fixed interaction strength ($U = 10t$) and varying density/ chemical potential (μ) for $\beta t = 2$.

annihilation operators for hole annihilation and creation operators respectively: $c_{\sigma i}^\dagger \rightarrow (-1)^i d_{\sigma i}$; $c_{\sigma i} \rightarrow (-1)^i d_{\sigma i}^\dagger$. A finite next nearest neighbor hopping term, t' , which we do not include in our discussion here, would break particle hole symmetry in Eq. 1.

We next calculate thermodynamic properties and the single-particle Green function by implementing the determinantal Quantum Monte Carlo (QMC) algorithm which essentially employs a Trotter-Suzuki decomposition to break up the non-commuting hopping and interaction terms in imaginary time τ .¹⁶⁻¹⁹ This maps the original 2D quantum problem to a (2+1)D classical problem where the extra dimension is set by the inverse temperature $\beta = 1/(k_B T)$. Details of the calculations and a discussion of the sign problem¹⁹⁻²¹ can be found in the supplementary material.

The compressibility $\kappa(U, \mu, T)$ is a useful diagnostic of the phases as it is zero in the Mott and band insulating phases (at $T = 0$) but non-zero in metallic and superconducting phases as shown in Fig 1 (a). κ is obtained from the fluctuation dissipation theorem:

$$\kappa n^2 = \frac{1}{N_s} \frac{d\langle \hat{N} \rangle}{d\mu} = \frac{\beta}{N_s} \left(\langle \hat{N}^2 \rangle - \langle \hat{N} \rangle^2 \right) \quad (2)$$

where $\langle \hat{N}^2 \rangle$ is given in terms of correlation functions $\langle \sum_{i,j} \hat{n}_i \hat{n}_j \rangle$ calculated directly using QMC techniques.

At half-filling, strong Coulomb interaction ($U/t \gg 1$) drives a phase transition from a metallic state to a Mott insulator (Fig 1) at a finite temperature T . At a fixed interaction strength, a Mott insulator to metal transition is driven by tuning the chemical potential, as seen by the behavior of κ in Fig 1(b); the agreement between κ obtained by fluctuation-dissipation and the numerical derivative of the density with respect to μ is a good check of our numerics.

For a finite U , at $n = 1$ the system is incompressible with $\kappa = 0$, as expected in a Mott insulator. Away from half filling in the metallic phase, the effect of strong interactions continues to dominate and is evident in the strong

suppression of κ as shown in Fig. 1 (b) The low compressibility can be understood as arising from a background of ‘‘Mott’’ sites (1 particle on every site) that essentially remain frozen and do not contribute to κ and only the excess doubly occupied sites (doublons) contribute to κ .

The main question we explore next is how the suppressed compressibility is reflected in the size of the Fermi surface as a function of interaction U and chemical potential μ .

Restructuring of the Fermi surface: From QMC we directly calculate the Green function in imaginary time τ and from that using an analytic continuation procedure we obtain the spectral function:

$$G_{\vec{k}}^r(\tau) = \int_{-\infty}^{\infty} \frac{e^{-\omega\tau}}{1 + e^{-\beta\omega}} A_{\vec{k}}^r(\omega) d\omega \quad (3)$$

The spectral function $A_{\vec{k}}^r(\omega) = -(1/\pi) \text{Im} G_{\vec{k}}^{ret}(\omega)$ gives information about the probability of finding an electron in state (\vec{k}, ω) . Fig. 2(a) shows the contour of the spectral function $A_{\vec{k}}^r(\omega = 0)$ over the Brillouin zone, and the locus of the spectral weight (black curve). A related quantity, the retarded Green’s function, defined by,

$$G_{\vec{k}}^{ret}(E) = \mathcal{P} \int_{-\infty}^{\infty} d\omega \frac{A_{\vec{k}}^r(\omega)}{\omega - E}, \quad (4)$$

provides a second indicator of the Fermi surface contour as $G_{\vec{k}}^{ret}(E = 0) = 0$ marks the boundary where the sign change occurs (shown in green). Here \mathcal{P} denotes the principal part of the integral.

Luttinger’s theorem asserts that the volume enclosed by the Fermi surface of an interacting Fermi liquid is proportional to the number of particles in the system.²² This allows us to find the reference non-interacting Fermi surface corresponding to the actual density obtained by QMC for the specific set of parameters (U, T, μ) (white contour in Fig. 2(a)).

It is also useful to compare with the contour obtained from the momentum distribution function (MDF) (Fig.

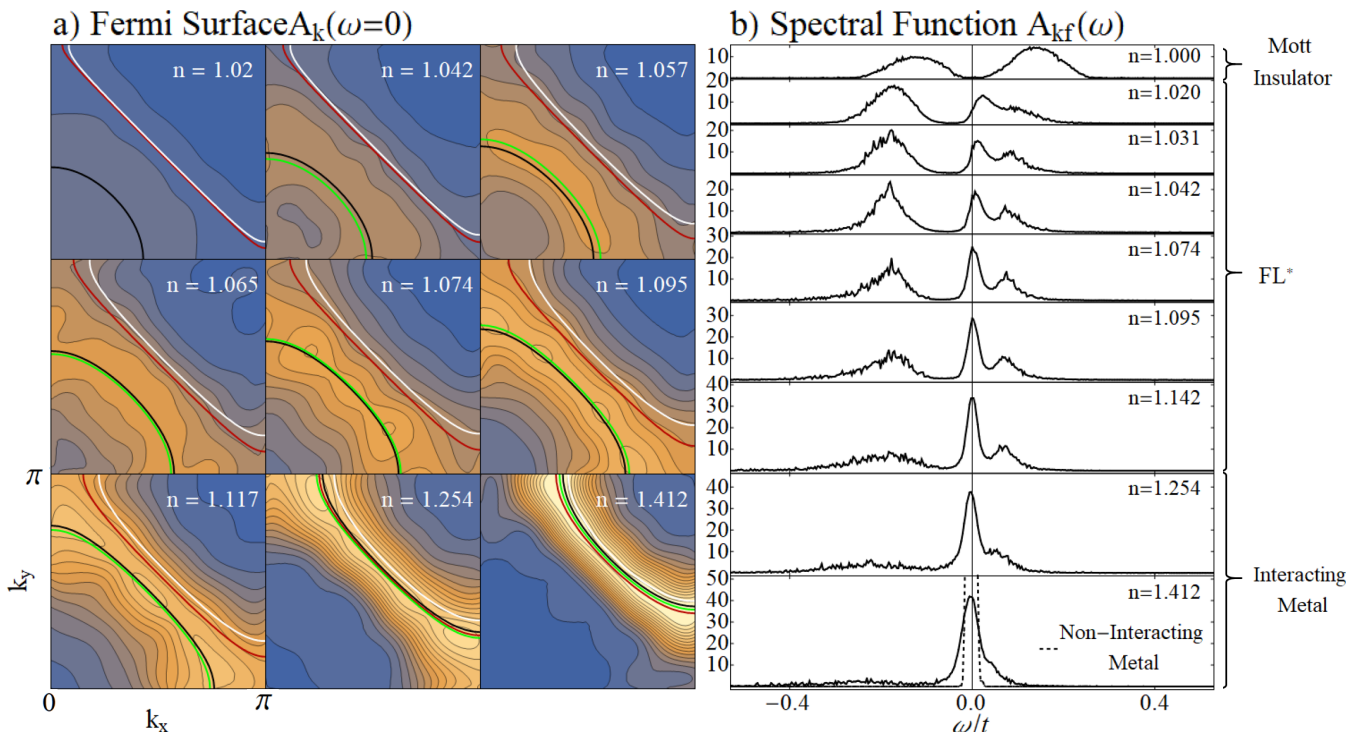


FIG. 2. a) The spectral weight, $A_{\vec{k}}(\omega = 0)$, in the Brillouin zone for a 16×16 site square lattice. We show different interpretations of the Fermi surface as contours. We have set interaction potential $U = 10t$ and $\beta t = 2$. Luttinger's Theorem applied to a free system (white); Momentum distribution function (MDF): the contour formed by $n_{\vec{k}} = 1/2$ (red); spectral weight at $A_{\vec{k}}(\omega = 0)$ (black); and retarded Green's function: $G_{\vec{k}}^{ret}(E) = 0$ (green). b) $A_{\vec{k}}(\omega)$ averaged over all k -states weighted by the value of $A_{\vec{k}}(\omega = 0)$ so to extrapolate the spectral function of the Fermi momentum. Total spectral weight is constant: $\frac{1}{\pi} \int_{-\infty}^{\infty} A_{\vec{k}}(\omega) d\omega = 1$. Thermal fluctuations broaden the spectral function an amount proportional to kT . The non-interacting metal spectral function at the same temperature (dashed) is contrasted with the interacting metal for $n = 1.412$

3(b)) $n_{\vec{k}} = 1/2$ calculated by QMC (shown in red in Fig. 2(a)). In the thermodynamic limit for a non-interacting system at $T = 0$, the MDF has a jump of size unity $Z = 1$ at the Fermi wave vector $k_F(\vec{k})$ when the system transitions from occupied states below k_F to zero occupancy above. In a Fermi liquid, following Luttinger's theorem, $k_F(\vec{k})$ does not change and $0 < Z \leq 1$. Due to inter-electron interactions, some of the states below $k_F(\vec{k})$ are scattered into states above but nevertheless in a Fermi liquid, a finite step at k_F persists at $T = 0$. At finite T , naturally the step gets rounded; however, from the peak in the gradient of the MDF (Fig. 3(b)) as a function of \vec{k} , we can extract the location of the underlying FS.

For doping greater than $p \gtrsim 0.2$ each of these methods of finding the FS show stark agreement. Such a validity of Luttinger volume is found even for large U for sufficiently large doping. However, when the doping is less than $p \lesssim 0.2$, we observe a departure of the FS contours obtained from these four methods. The size of the red and white surfaces, corresponding to the $n_{\vec{k}} = 1/2$ contour and the Luttinger surface respectively, count the total electronic density. The spectral weight and retarded Green's function boundaries, black and green contours respectively, on the other hand recede to include fewer

states. In other words, the spectral function methods indicate that the Fermi surface reconstructs from enclosing $n = 1 + p$ fermions to a smaller FS, shown in Fig 3(a) as the deviation of the Fermi surface area from the dashed curve. As observed in Fig. 2 (a), the black and green contours transform from being close to a diamond shaped Fermi surface to a small circular Fermi surface centered around the Γ point; the deviation occurs for densities $n \lesssim 1.2$.

The metallic weight or the quasiparticle weight, shown in Fig 3 (a), shows the percentage of the spectral function, $A_{\vec{k}_f}(\omega)$, inside the bounds of the non-interacting metal, defined by

$$MW = \frac{1}{\pi} \int_{-\epsilon}^{\epsilon} A_{\vec{k}_f}(\omega) d\omega \quad (5)$$

where as a reference we use the $U = 0$ spectral function of the thermally broadened non-interacting metal from a delta function to a Lorentzian distribution of width 2ϵ in Fig 2 (b) (lowest panel).

The interacting system shows the development of incoherent side bands or Mott bands around the peaked spectral function at $\omega = 0$. The Fermi surface restructuring is already visible below $n \approx 1.2$ and the deviation

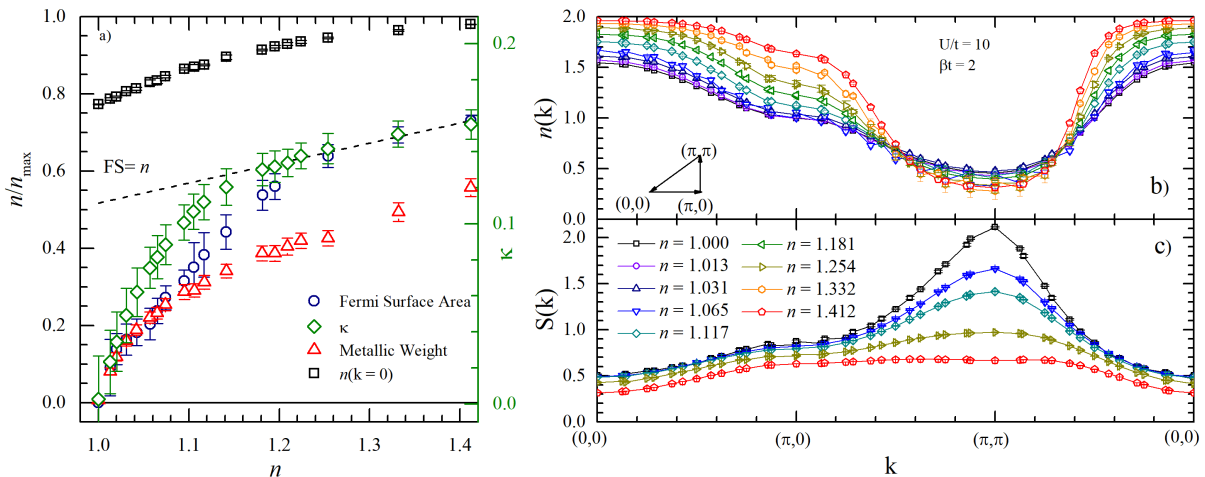


FIG. 3. a) We calculate the number of particles enclosed by the (black) Fermi surface in Figure 2, the occupation of the $n_{\vec{k}} = (0, 0)$ state, and the metallic weight, defined in equation 5. The occupation of the $\vec{k} = (0, 0)$ state in the highly interacting regime is strongly dependent on the average density. The area of the Fermi surface, according to Luttinger's theorem, is proportional to the density. Turning on strong interactions decreases the size of the Fermi surface for doping around 0, contradicting this rule. b) The density as a function of momentum is plotted for multiple values of n . The Fermi surface is noticeable for larger densities. c) Spin Spin correlations across the Brillouin zone show spin ordering in the Mott limit and the highly interacting metallic limit.

of the actual Fermi contour from the Luttinger contour only gets more pronounced as the incoherent weight increases upon approaching the Mott transition at $n = 1$.

It is important to note that there is no evidence of long range anti-ferromagnetic order at the temperatures and parameters we are analyzing the Fermi surface. The spin structure factor at (π, π) , shown in Fig 3 (c), shows a small peak at $n = 1$ which gets quickly suppressed as the density moves away from this commensurate value.

Discussion and Outlook:

Our results suggest that if secondary ordering in the spin, charge or pairing channel is suppressed, the proximity to a Mott insulator alone drives the reconstruction of the Fermi surface. Featureless doped quantum spin liquids are perhaps the most promising platform for the observation of such a state of matter. Sachdev, Senthil and collaborators have proposed the possibility of a non-Fermi liquid phase (dubbed FL*) with a Fermi surface composed of fractionalized spinons with a volume $(n - 1) \bmod 2$.¹⁵ They claim that quantum fluctuations of the antiferromagnetic order parameter generate emergent gauge fields that lead to a new state of matter with topological order^{23,24}. Such an FL* phase with a reconstructed Fermi surface could be a possible description of the pseudogap phase²⁵. Our results on the Hubbard model are the first indication of such an FL* phase from a controlled calculation with only statistical errors. Going forward, further simulations are necessary to study an extended Hubbard model with nearest neighbor hopping to describe the more realistic parameters for the cuprates. Here our aim was to show the emergence of the FL* phase in the very simplest case with only nearest neighbor hopping. It would also be interesting to push

the calculations to even lower temperatures to see the emergence of the superconducting phase from the FL* phase for doping values p below p_c^{PG} and contrast that with the superconducting phase that emerges from the FL phase above this critical value.

Acknowledgments: We acknowledge useful discussions with Hasan Khan during the initial stages of this project. I.O. and N.T. acknowledge the support of the DOE-BES Grant No. DE-FG02-07ER46423. T. P. acknowledges support from CNPq, FAPERJ and INCT on Quantum Information.

REFERENCES

- 1 S. Badoux, W. Tabis, F. Laliberté, G. Grissonnanche, B. Vignolle, D. Vignolles, J. Béard, D. A. Bonn, W. N. Hardy, R. Liang, N. Doiron-Leyraud, L. Taillefer, and C. Proust, *Nature* **531**, 210–214 (2016).
- 2 N. Bulut, D. Scalapino, and S. White, *Phys. Rev. B* **50**, 7215 (1994).
- 3 R. Preuss, W. Hanke, and W. von der Linden, *Phys. Rev. Lett.* **75**, 1344 (1995).
- 4 A. Moreo, S. Haas, A. W. Sandvik, and E. Dagotto, *Phys. Rev. B* **51**, 12045 (1995).
- 5 C. Huscroft, M. Jarrell, T. Maier, S. Moukouri, and A. N. Tahvildarzadeh, *Phys. Rev. Lett.* **86**, 139 (2001).
- 6 M. Civelli, M. Capone, S. S. Kancharla, O. Parcollet, and G. Kotliar, *Phys. Rev. Lett.* **95**, 106402 (2005).
- 7 E. Gull, M. Ferrero, O. Parcollet, A. Georges, and A. J. Millis, *Phys. Rev. B* **82**, 155101 (2010).
- 8 T. A. Maier, T. Pruschke, and M. Jarrell, *Phys. Rev. B* **66**, 075102 (2002).
- 9 K.-S. Chen, Z. Y. Meng, T. Pruschke, J. Moreno, and M. Jarrell, *Phys. Rev. B* **86**, 165136 (2012).

- ¹⁰ S. Sakai, Y. Motome, and M. Imada, *Phys. Rev. Lett.* **102**, 056404 (2009).
- ¹¹ J. E. Gubernatis, M. Jarrell, R. N. Silver, and D. S. Sivia, *Physical Review B* **44**, 6011 (1991).
- ¹² A. W. Sandvik, *Physical Review B* **57**, 10287 (1998).
- ¹³ M. Jarrell and J. E. Gubernatis, *Physics Reports* **269**, 133 (1996).
- ¹⁴ K. Bouadim, Y. L. Loh, M. Randeria, and N. Trivedi, *Nature Physics* **7**, 884–889 (2011).
- ¹⁵ T. Senthil, S. Sachdev, and M. Vojta, *Phys. Rev. Lett.* **90**, 216403 (2003).
- ¹⁶ R. Blankenbecler, D. J. Scalapino, and R. L. Sugar, *Physical Review D* **24**, 2278 (1981).
- ¹⁷ J. E. Hirsch, *Physical Review B* **31**, 4403 (1985).
- ¹⁸ S. R. White, D. J. Scalapino, R. L. Sugar, E. Y. Loh, J. E. Gubernatis, and R. T. Scalettar, *Physical Review B* **40**, 506 (1989).
- ¹⁹ R. R. dos Santos, *Brazilian Journal of Physics* **33**, 36 (2003).
- ²⁰ E. Y. Loh, J. E. Gubernatis, R. T. Scalettar, S. R. White, D. J. Scalapino, and R. L. Sugar, *Physical Review B* **41**, 9301 (1990).
- ²¹ V. I. Iglovikov, E. Khatami, and R. T. Scalettar, *Physical Review B* **92**, 045110 (2015).
- ²² J. M. Luttinger, *Phys. Rev.* **119**, 1153 (1960).
- ²³ M. S. Scheurer, S. Chatterjee, W. Wu, M. Ferrero, A. Georges, and S. Sachdev, *Proceedings of the National Academy of Sciences* **115**, E3665–E3672 (2018).
- ²⁴ D. G. Joshi, C. Li, G. Tarnopolsky, A. Georges, and S. Sachdev, “Deconfined critical point in a doped random quantum heisenberg magnet,” (2019), arXiv:1912.08822 [cond-mat.str-el].
- ²⁵ W. Wu, M. S. Scheurer, S. Chatterjee, S. Sachdev, A. Georges, and M. Ferrero, *Physical Review X* **8** (2018), 10.1103/physrevx.8.021048.

Supplement to Topological Fermi-surface Reconstruction in the Repulsive Fermi-Hubbard Model

Ian Osborne¹, Thereza Paiva², and Nandini Trivedi¹

(1) *Department of Physics, The Ohio State University, Columbus, OH 43210, USA and*

(2) *Instituto de Física, Universidade Federal do Rio de Janeiro, Caixa Postal 68.528, 21941-972, Rio de Janeiro, RJ, Brazil*

(Dated: July 28, 2022)

I. DETAILS ABOUT THE SIMULATIONS

In Determinantal Quantum Monte Carlo (DQMC) the grand partition function is expressed as a sum over all Ising spin configurations $c \equiv \{s\}$ at each space-time lattice point, of a product of determinants.

$$\mathcal{Z} = \left(\frac{1}{2}\right)^{L^d M} \text{Tr}_{\{s\}} \det O^\uparrow(\{s\}) \cdot \det O^\downarrow(\{s\}) \quad (1)$$

where $M = \beta/\Delta\tau$, L is the linear size of the system and d the dimension. The ‘‘Boltzmann weight’’ is given by the product $p(c) = \det O^\uparrow(\{s\}) \cdot \det O^\downarrow(\{s\})$ which is not always positive. We can keep track of the sign by writing

$$p(c) = \text{sign}(c) |p(c)|, \quad (2)$$

where $\text{sign}(c) = \pm 1$, this way the absolute value is used as the weight in the Monte Carlo procedure and the sign is included in the measurements. Any expectation value $\langle A \rangle$ is then given by

$$\langle A \rangle = \frac{\sum_c p(c) A(c)}{\sum_c p(c)} = \frac{\sum_c |p(c)| \text{sign}(c) A(c)}{\sum_c |p(c)| \text{sign}(c)} \equiv \frac{\langle \text{sign} A \rangle}{\langle \text{sign} \rangle}. \quad (3)$$

At low temperatures, both $\langle A \text{ sign} \rangle$ and $\langle \text{sign} \rangle$ become very small, leading to the well known ‘‘fermion sign problem’’. The fermion sign problem is also known to get worse with increasing system size as is shown in figure 1. We have then restricted our system sizes to lattices up to 16×16 , where $\langle \text{sign} \rangle > 0.5$.

One sweep of DQMC constitutes the metropolis algorithm attempting to flip the Ising spin on every site on the square lattice and for every time slice. 1000 warm up sweeps are sufficient to reach equilibrium, while 15000 sweeps are used for measuring thermodynamic quantities with the associated error bars. For the $(2+1)$ D lattice, we use $\Delta\tau = 1/40$ and $M = 80$ imaginary time slices, which gives $\beta t = M\Delta\tau = 2$ and a temperature $T = 0.5t$. The interaction potential is held constant at an order of magnitude greater than t : $U = 10t$.

We average the results from seven trials to increase statistics. Four of these trials are conducted on a 16×16 cluster, three on a 14×14 cluster. The two lattice sizes compliment by providing data for k -states that are in-accessible by either lattice size individually. The different lattice sizes affect quantities like density and compressibility to a negligible degree.

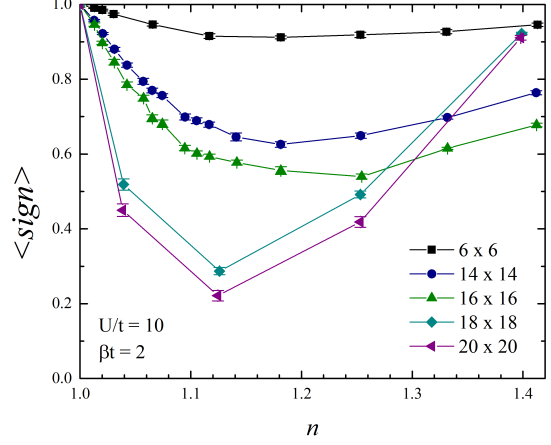


FIG. 1. a) Average total sign as a function of density for lattice sizes from 6×6 to 20×20 . Temperature is set such that $\beta t = 2$, and the interaction potential is $U = 10t$.

II. COMPRESSIBILITY

The compressibility, calculated from the Fluctuation Dissipation Theorem, is used as a diagnostic for metallic phases. In Fig. 2 the compressibility of a non-interacting ($U/t = 0$) and interacting ($U/t = 7$) system are compared for a cluster size of 6×6 and temperature of $T = t/2$.

We posit that at large interaction values there is a background of Mott sites, on which the charge carriers are essentially the doublons or holes depending on whether the density is higher than unity or lower, with a density of $p = \text{mod } n - 1$. Using this assumption, we notice that for large interaction strengths, around half filling the compressibility is suppressed due to a lack of charge carrying doublons or holes and the system becomes a Mott insulator. For fillings close to 2, the compressibility should approach zero as the band gets fully filled and the system becomes a band insulator.

Both of these claims are confirmed by Fig. 2. Another non-trivial check of our assumption is that the compressibility of the strongly-interacting system at $n = 1 + p = 1.5$ should be approximately half the compressibility of the non-interacting system at $n = 1$: $\kappa(U/t \gg 1, p = 0.5) \approx \frac{1}{2} \kappa(U/t = 0, p = 0)$. This is because the approximate density of charge carriers in the non-interacting case

at $n = 1$ is twice the approximate density of charge carriers in the strongly-interacting case at $n = 1.5$ ($p = 0.5$). This is also confirmed by Fig. 2.

III. METHODS FOR COMPUTING THE FERMI SURFACE

All methods used for computing the Fermi surface derive from the Green's function, $G_{\vec{k}}(\tau) = \langle c_{\vec{k}}^\dagger(\tau)c_{\vec{k}}(0) \rangle$. This correlation is calculated for each discrete $\tau \in [0, 80]$ imaginary time step. The section *Fermi surface restructuring* describes how different quantities are used to construct the Fermi surface; here we will present how these quantities are calculated using the Green's function.

A. Luttinger's Theorem applied to a free system

The size for the Fermi surface is proportional to the total particle number N , from Luttinger's theorem. We calculate the non-interacting/tight binding contour in k -space N particles

$$N = \sum_{\vec{k}} G_{\vec{k}}(0) \quad (4)$$

B. Momentum distribution function (MDF)

The MDF is calculated with the following identity

$$n_{\vec{k}} = G_{\vec{k}}(0) \quad (5)$$

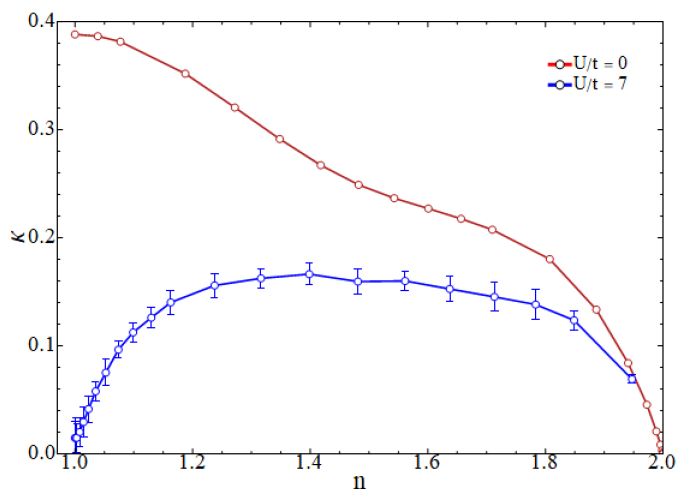


FIG. 2. Compressibility for a strongly interacting system and a non-interacting system, at $T = t/2$ and for a 6×6 lattice.

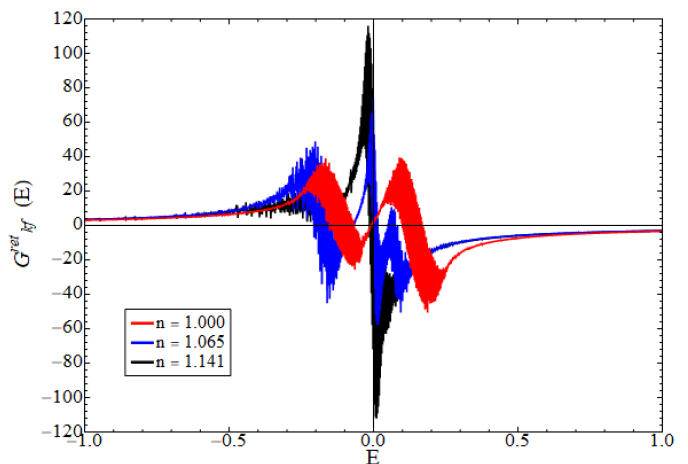


FIG. 3. The retarded Green's function: $G_{k_f}^{ret}(E)$ as a function of E . Each curve is 0 at $E = 0$ within an uncertainty term.

We find the contour, $n_{\vec{k}} = 1/2$, which defines the surface which encloses the k -states that are more likely to be filled than not.

C. Spectral weight at $A_{\vec{k}}(\omega = 0)$

In the non-interacting and thermodynamic limits the only k -states that have spectral weight at $\omega = 0$ are the states on the Fermi surface. We use this property to find the size of the Fermi surface by examining the k -states that have spectral weight at $\omega = 0$.

The Green's function- Spectral function relationship is described in equation 6. We implement an iterative maximum entropy method to calculate the spectral function that most accurately reproduces the input Green's function within error bars.

$$G_{\vec{k}}(\tau) = \int_{-\infty}^{\infty} \frac{e^{-\omega\tau}}{1 + e^{-\beta\omega}} A_{\vec{k}}(\omega) d\omega \quad (6)$$

The Fermi surface is constructed by finding the energy value that maximizes the function $A_{E(\vec{k})}(\omega = 0)$, where $E(\vec{k})$ is the tight binding dispersion: $E(\vec{k}) = -2t(\cos k_x + \cos k_y)$. We take this energy to be E_f and create a tight binding contour to approximate the Fermi surface.

The spectral function at the Fermi wave-vector is constructed by averaging the spectral function for each momentum statistically weighted by $A_{\vec{k}}(\omega = 0)$:

$$A_{k_f}(\omega) = \sum_{\vec{k}} A_{\vec{k}}(\omega) A_{\vec{k}}(\omega = 0) / \sum_{\vec{k}} A_{\vec{k}}(\omega = 0) \quad (7)$$

Although seemingly arbitrary, we construct the spectral function at the Fermi wave vector this way because of its relevance in the non-interacting/thermodynamic limit which exactly gives the spectral function at k_f .

D. Retarded Green's function

$$G_{\vec{k}}^{ret}(E) = \mathcal{P} \int_{-\infty}^{\infty} d\omega \frac{A_{\vec{k}}(\omega)}{\omega - E} \quad (8)$$

The retarded Green's function is calculated using the

spectral function in equation 8, $G_{\vec{k}}^{ret}(0)$. We construct the Fermi surface by finding the contour $G_{\vec{k}}^{ret}(0) = 0$. Fig. 3 shows $G_{k_f}^{ret}(E)$ for Fermi-wave vectors for three different densities. Each curve is zero for $E = 0$ which is a non-trivial check that our calculation of $A_{k_f}(\omega)$ in section C is accurate.